A Simple and Inexpensive Filtration Method for the Preparation of LiFePO$_4$/C Powders

Jing-Ting Kuo, Hong-Kai Yang and Jenn-Shing Chen[*]

Department of Applied Chemistry, National University of Kaohsiung, Kaohsiung City, Taiwan 811, R.O.C.
[*]E-mail: jschen@nuk.edu.tw

LiFePO$_4$/C composites are synthesized using a simple and inexpensive filtration method. Organic filter templates composed of porous polycarbonate, mixed-cellulose, and cellulose are used as sacrificial hard templates. The LiFePO$_4$/C composites are prepared by infiltrating LiFePO$_4$ precursor solutions into the organic filter templates. Once the organic filter templates are removed by calcination, the LiFePO$_4$ featured meso/macroporous and nanowire structures with residual carbon. All samples are characterized using XRD, SEM/EDS, TEM, EA, BET surface area, CV, EIS, and charge-discharge tests. The characterization data reveal that the organic filter templates provide a specific pore structure that can lead to an increase in the conductivity of LiFePO$_4$. The best performing LiFePO$_4$/C prepared from cellulose (C-700) provides a uniform particle size of 100-150 nm. The particle sizes uniformity can be ascribed to the effect of the structure of 3D fibers in the cellulose on dispersing the LiFePO$_4$ particles and reducing particle aggregations. LiFePO$_4$/C prepared from cellulose thus has a higher discharge capacity and improved rate capability, with 157 mAh g^{-1} at 0.1C and 112 mAh g^{-1} at 10C. We demonstrate that the LiFePO$_4$/C composites from appropriate organic filter templates can provide excellent electrochemical performance.

Keywords: Lithium iron phosphate, Template method, Lithium-ion battery, Cathode material

1. INTRODUCTION

In the past decade, lithium iron phosphate (LiFePO$_4$) has been studied extensively for Li-ion batteries as a cathode material due to its high theoretical capacity (170 mAh g^{-1}), good cyclability, relatively low cost, and environmental benign nature. These significant advantages make LiFePO$_4$ a good candidate for use in large scale Li-ion batteries for electric vehicle (EV) and hybrid electric vehicle (HEV) applications [1-4]. However, its poor rate capability places limitations on its practical

applications. This poor rate performance is mainly caused by its intrinsic low electronic conductivity ($\sim 10^{-9}$ S cm^{-1}) and the slow kinetics of Li$^+$ diffusion through the LiFePO$_4$/FePO$_4$ interface [3, 5-8]. Considerable efforts have been made over the years to overcome this drawback involving optimizing synthetic processes [1, 2, 8-13], carbon nanocoating [14-18], particle-size minimization[6, 16, 17, 19], the addition of metal powders [8, 20, 21], doping with supervalent ions [1, 3, 22-24] or carbothermal formation of the surface conducting phase [8, 15, 19, 25-27].

The electrochemical properties of LiFePO$_4$ can be improved by the coating with carbon to form LiFePO$_4$/C composites [8, 27-29]. The performance of LiFePO$_4$/C composites relies on the morphology and particle size of the active material, the structure of the carbon precursor, the amount of carbon content, the form of carbon contact, and the mixing and sintering recipe. Previous studies have been examined the behavior of LiFePO$_4$/C composites in terms of their carbon structural parameters originate in the Raman studies [30-34], finding that the choice of suitable organic precursors as a carbon source is very important for tailoring the final properties of carbon coated composite powders. In this study, various organic templates were used as carbon sources to synthesize the LiFePO$_4$/C composites.

Hard template synthesis has been widely applied to many metal oxide systems for the preparation of high-surface area metal oxide derivatives (nanoparticles or nanostuuctures) [32, 33, 35-39]. The synthetic manipulation includes three major steps: (i) infiltration of the template porosity with a precursor solution; (ii) heat treatment of the impregnated template; (iii) removal of the template framework to form the product. Sakatomo et al. [40] first reported the synthesis of V$_2$O$_5$ electrode materials with pores ranging from 10 ~ 30 nm for lithium ion batteries via the hard-template method in 2002. They demonstrated that the small pores of V$_2$O$_5$ exhibited higher capacities at higher discharge rates owing to improved charge transport. Since then, a number of studies have investigated the use of silica or carbon hard-templates to prepare many other electrode materials with a range of pore sizes including SnO$_2$, LiNiO$_2$, TiO$_2$, Li$_4$Ti$_5$O$_{12}$, LiMn$_2$O$_4$, LiFePO$_4$, and porous carbon for use in batteries or capacitors [41-46]. Moreover, several recent review articles have described the preparation of electrode materials for lithium-ion batteries using the template method [47-49]. This work applied the concept of exotemplating. Exotemplates are extended structures that contain voids which provide space for the formation of a divided solid. This technique is also called "confined space synthesis" or "compartment solidification" [37].

Sol-gel and nanocasting templating methodes were used to prepare LiFePO$_4$/C composites. Usually, both porous silica and carbon are used as hard-templates through a wetness impregnation technique [42]. However, LiFePO$_4$ could not be templated directly through a silica monolith because it dissolves when washed with HF during the silica template removal, or chemically reacts when washed with NaOH. In addition, LiFePO$_4$ could not be templated with a carbon monolith because removal of the carbon template in the presence of oxygen caused the LiFePO$_4$ to oxidize into Li$_3$Fe$_2$PO$_4$ and other impurity phases [42]. Therefore, various organic templates were selected as sacrificial hard templates to form porous LiFePO$_4$/C composites, allowing for the specific tailoring of the pore size. This permits to make study of the effects of morphological changes on the electrochemical performance in relationship to the organic templates. The LiFePO$_4$/C composites were synthesized by infiltrating the lithium iron phosphate precursor solutions into the organic templates. While the organic templates

were removed by calcination, the LiFePO$_4$ featured meso/macroporous and nanowire structures with residual carbon from the decomposition of the organic template. Recently, Jugovic et. al [46] reported the preparation of a LiFePO$_4$/C composite using the cellulose matrix-assisted method. They used filter paper as a template and a carbon source to synthesize LiFePO$_4$/C composites. In their report, the filtration method offered a new examination of the crystal growth of LiFePO$_4$ and a fast preparation for LiFePO$_4$/C powders.

In the present work, we applied the filtration method and used various organic filters of porous polycarbonate, mixed-cellulose and cellulose fibers as sacrificial hard templates for the preparation of LiFePO$_4$/C particles. A series of morphological changes of LiFePO$_4$/C composites originating from the various organic hard templates were documented and characterized. Electrochemical properties of composites were evaluated from cyclic voltammogram (CV) and charge-discharge cycling tests.

2. EXPERIMENTAL

The sol-gel method was applied for the synthesis of the electrode precursor solution. Accordingly, LiOH•H$_2$O (TEDIA), Fe(NO$_3$)$_3$•9H$_2$O (Riedel-deHaen), H$_3$PO$_4$ (J.T. Baker), and Ethylene Glycol (J.T. Baker) were used to create the LiFePO$_4$ precursor solution. The LiFePO$_4$ solution was prepared using water-based solution chemistry, and the precursors were selected so that the solution would not precipitate prior to infiltration. The precursor solution was prepared using ferric nitrate, lithium hydroxide and phosphoric acid in proportions for a 1:1:1 molar ratio. Commercially available porous polycarbonate (Millipore, pore diameters of 100 nm), mixedcellulose (ADVANTEC, pore diameters of 200, 450 and 800 nm) and cellulose (Whatman, pore diameter of 700 nm) filters were used as hard templates for the synthesis of LiFePO$_4$/C composites. These hard templates were impregnated with the precursor solution of 1M LiFePO$_4$ until incipient wetness was attained. The impregnated sample was dried at 100 $^{\circ}$C. The impregnation-drying cycle was repeated up to four times with a vacuum filtration apparatus to increase the amount of active material in the sample. The impregnated samples were dried in air at 350°C for 30 minutes and then calcined in a reducing gas atmosphere (Ar/H$_2$ = 95/5) at 600°C for 12 h to yield LiFePO$_4$/C composite powders. This procedure yields the Fe(II) oxidation state necessary for LiFePO$_4$ and decomposes the template into the residual carbon for improved conductivity.

The structures of the as-prepared samples were observed by powder X-ray diffraction (XRD) analysis performed using a Rigaku-D/MaX-2550 diffractometer with Cu K$_\alpha$ radiation (λ=1.54 Å). Sample morphology was examined using a scanning electron microscope (SEM, S-4300, Hitachi Co.) and transmission electron microscope (TEM, JEN-2010, JEOL Co.). Nitrogen adsorption-desorption isotherm was measured using ASAP2020 (Micromeritics, USA). The specific surface area was calculated by the Brunauer-Emmett-Teller (BET) method. The pore size distribution was analyzed using the Barrett-Joyner-Halenda (BJH) method from the adsorption branch. The residual carbon content for the samples was determined by an automatic elemental analyzer (Elementar vario, EL III).
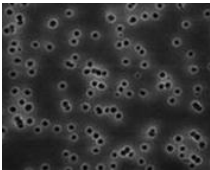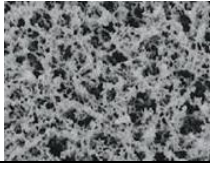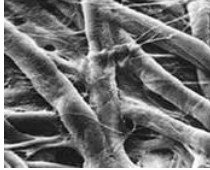
Electrode fabrication and coin cell assembly were carried out as reported in our previous work [50]. In brief, the as-prepared LiFePO$_4$/C was mixed with 5wt% acetylene black, 5wt% SFG-6

synthetic flake graphite (Timcal Ltd.), and 10wt% polyvinylidene fluoride (PVDF) binder (MKB-212C, Elf Atochem) and then was stirred for 20 minutes at room temperature with a magnetic bar, and then with a turbine for 5 minutes at 2000 rpm. The cathode was achieved by coating the mixture onto a piece of aluminum foil and then dried at $120^{\circ}C$ for 40 min. Electrodes were dried in a vacuum oven at $120^{\circ}C$ for overnight before cell assembly. Coin cells were assembled with the prepared cathode, lithium anode, Celgard 2400 polypropylene separator and 1 M $LiPF_6$ in an ethylene carbonate/dimethyl carbonate (EC/DMC) electrolyte. The CV test was performed at a scan rate of 0.1 mV s^{-1} in voltage range from 4.2 to 2.5 V. The galvanoststic charge-discharge measurements were carried out at a constant current of 0.5C in the potential range from 2.5 to 4.2 V at room temperature. It is noted that the specific capacity was calculated based on the mass of active material in the electrode.

3. RESULTS AND DISCUSSION

According to previous reports [12, 22, 25, 51, 52], the preparation of carbon-coated $LiFePO_4$ ($LiFePO_4$/C) with small particle sizes could improve the capacity and the limited rate capability of $LiFePO_4$. Here we report the preparation of nano-crystalline $LiFePO_4$/C composite powders obtained using the hard template technique. Three different organic filter templates, polycarbonate (P-100), mixed-cellulose (M-200), and cellulose (C-700), were used as sacrificial hard templates to produce porous $LiFePO_4$/C composites with the specific pore structures as shown in Table 1.

Table 1. $LiFePO_4$/C samples processed with various templates and their corresponding specifications.

Template type	Template photograph[53, 54]	Samples	Pore size of templates (nm)
Polycarbonate		P-100	100
Mixedcellulose		M-200	200
Cellulose		C-700	700

The effects of morphological changes on the electrochemical performance and the physical properties of the $LiFePO_4$/C composites were studied. Photographs of these organic templates and their

pore diameters are presented in Table 1. The color of all prepared $LiFePO_4/C$ powders exhibited deep black, in contrast to the gray color of $LiFePO_4$ powders.
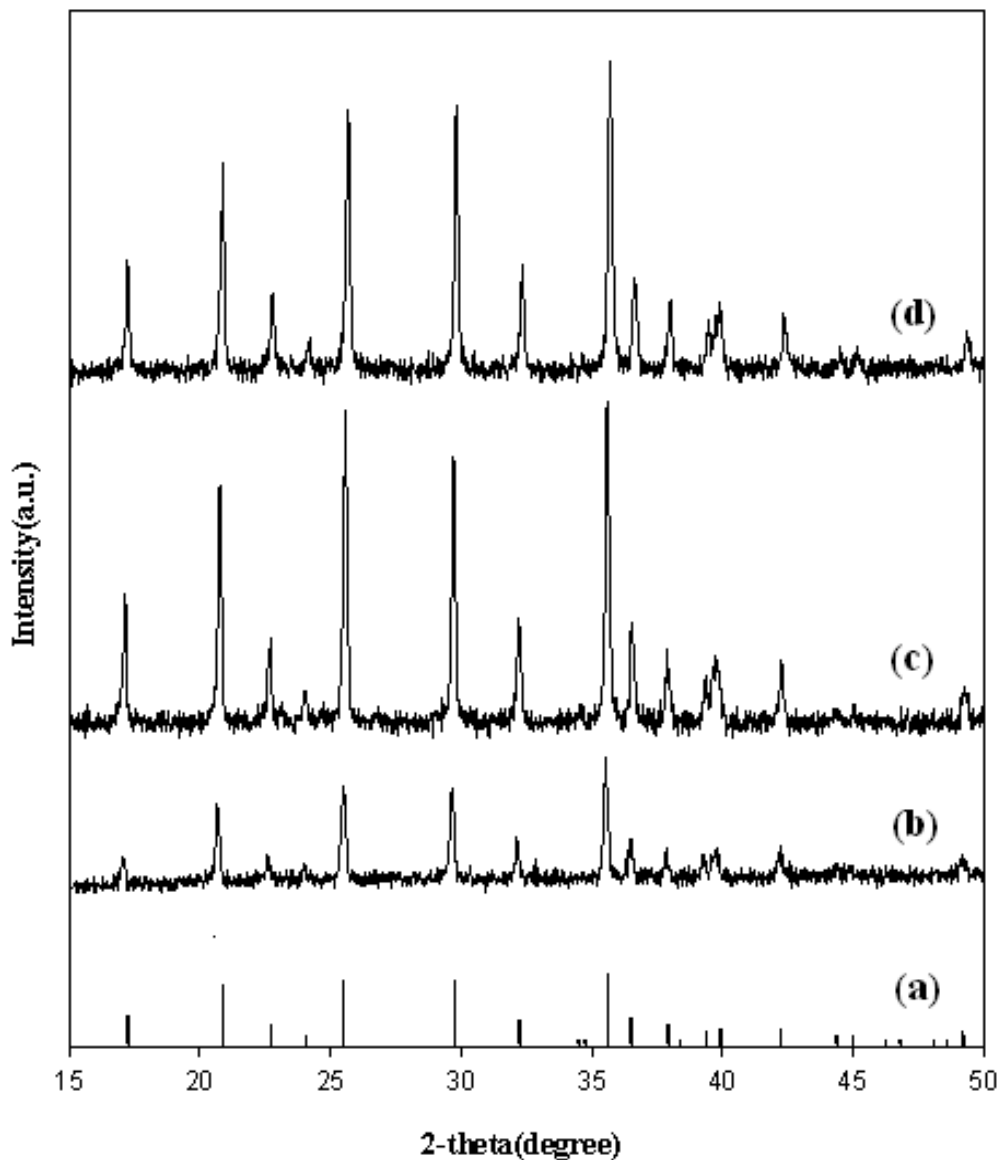
Figure 1. X-ray diffraction patterns of (a) theoretical $LiFePO_4$(JCPDS card no.40-1499)); (b) P-100; (c) M-200; (d) C-700.

Fig. 1 shows XRD patterns of the $LiFePO_4/C$ synthesized powders with different organic templates. All peaks can be indexed as pure and well-crystallized $LiFePO_4$ phase with an ordered olivine structure and a space group of orthorhombic *Pnmb*. As can be seen from the XRD curves shown in Fig. 1, there are no any evidence of the formation of crystalline or amorphous carbon. It seems that organic templates were used as carbon source most likely remains amorphous or as low crystalline carbon in the final product.

The morphology of the $LiFePO_4/C$ composites prepared using P-100, M-200, and C-700 as temples were examined using SEM and TEM, as shown in Fig. 2.
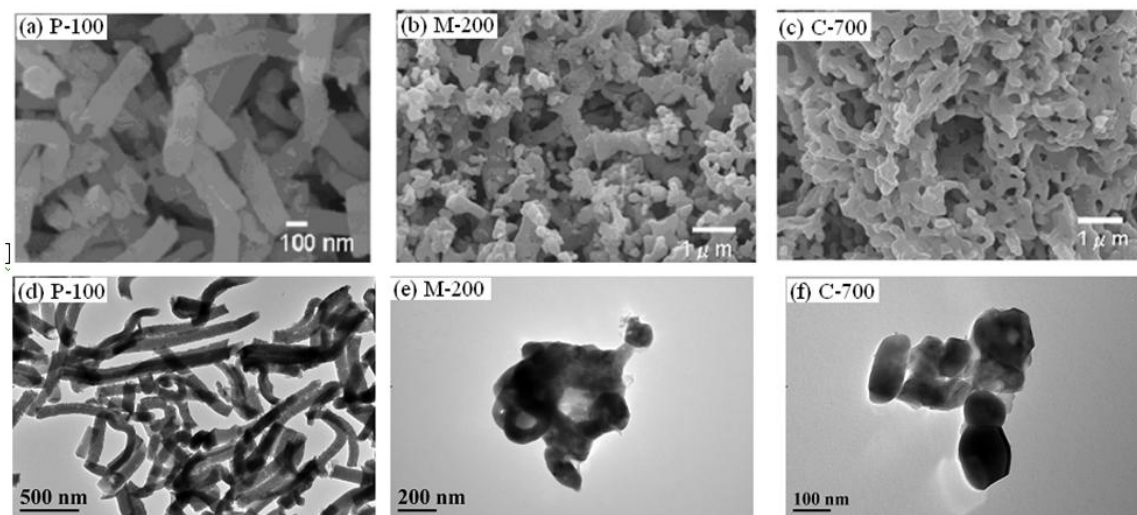
**Figure 2.** SEM images of LiFePO$_4$/C (a) P-100; (b) M-200; (c) C-700 and TEM images of LiFePO$_4$/C (d) P-100; (e) M-200; (f) C-700.

The general appearance of LiFePO$_4$/C composites prepared using the P-100 template displays a fibrous morphology with smooth surface and uniform diameter of 150 nm (Fig. 2(a), (d)). The porosity of P-100 polycarbon template is made up of mesopores measuring 100 nm in diameter. Obviously, the LiFePO$_4$/C nanofibers are a replica of one-dimensional (1D) channeled mesoporous P-100. The diameters of the LiFePO$_4$/C nanofiber replicas (~150 nm) are larger than that of the host P-100 (100 nm), which may result from the decomposition of the organic filter templates into residual carbon, which is then coated on the surface of LiFePO$_4$ fibers during pyrolysis. The typical morphology of the mixed-cellulose and cellulose is three-dimensional (3D) interconnected mesopores and macropores. The morphology of LiFePO$_4$/C prepared from M-200 and C-700 hosts exhibits well-developed interconnected mesopores and macropores (Fig. 2(b)-(c), (e)-(f)). These meso- and macro-pores allow the organic electrolyte to enter the material and access the high interfacial areas, which may improve the charge transport and power capability. The particle size of the LiFePO$_4$/C produced from M-200 is in the 70 – 200 nm range, which is in good agreement with the cavity size of M-200 mixed-cellolose (about 200 nm). Although the porosity of the C-700 cellulose template has a larger pore size of about 700 nm, the LiFePO$_4$/C prepared from C-700 provides a uniform particle size within the 100-150 nm range (Fig. 2(f)). The uniform particle sizes can be ascribed to the effect of the structure of 3D fibers in the cellulose in dispersing the LiFePO$_4$ particles and reducing the particle aggregations. Fig.3 exhibits SEM images of the prepared LiFePO$_4$/C composites and the corresponding EDS spectra. It can be seen from the SEM images that the particles for all samples could be composed of a secondary particle containing many smaller sized particles.
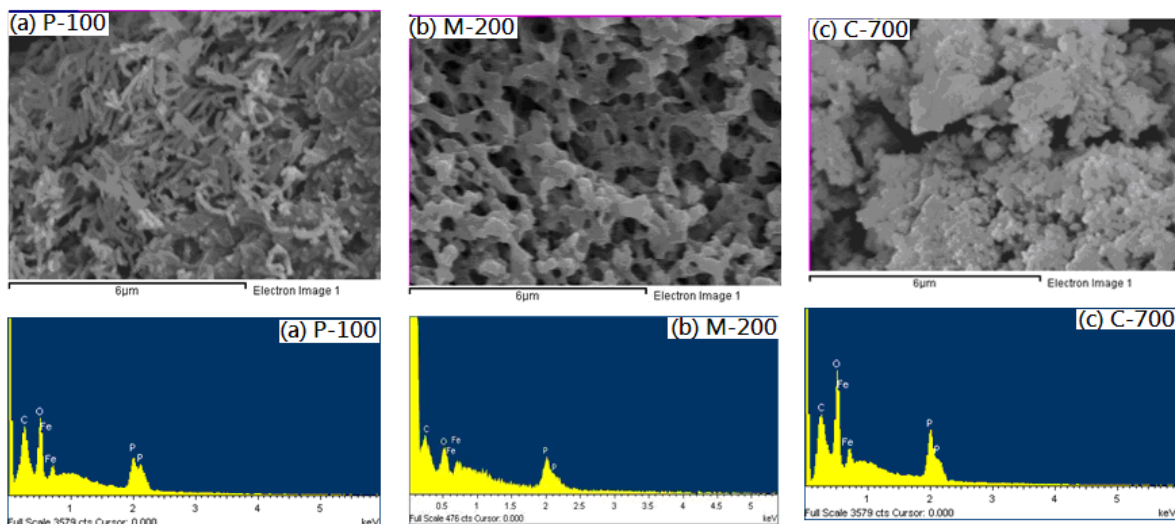
Figure 3. SEM images of LiFePO$_4$/C and the corresponding EDS spectra for (a) P-100; (b) M-200; (c) C-700.
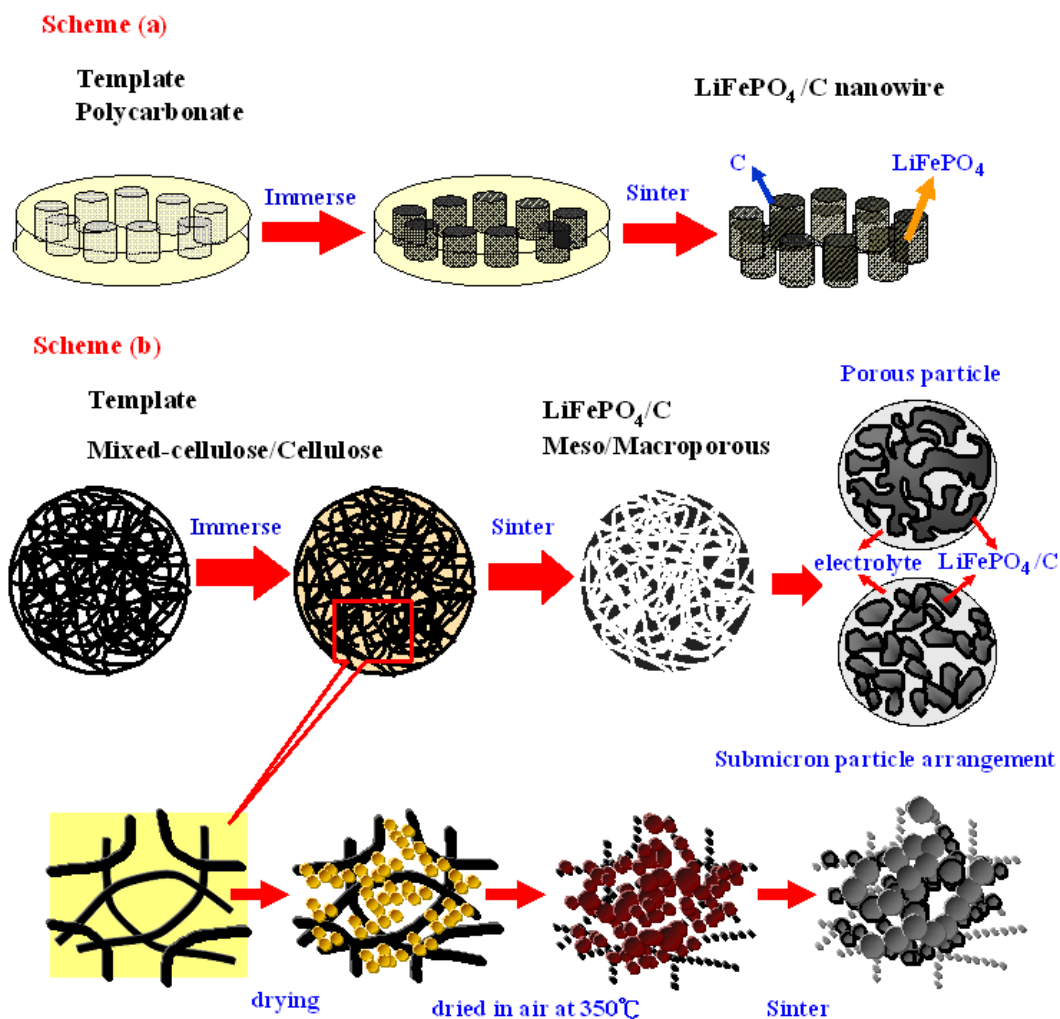
Figure 4. Schematic of the synthesis of (a) nanowires LiFePO$_4$/C by using polycarbonate template and (b) porous LiFePO$_4$/C by using mixed-cellulose or cellulose templates.

The EDS spectra result of LiFePO$_4$/C composites unambiguously confirmed that the particles in the selected region possessed Fe, P, O, and C components.

To prepare the various shapes of LiFePO$_4$/C, a clear solution consisting of LiFePO$_4$ precursors was incorporated into the different morphologies of organic filter templates using an impregnation method. The specific morphology of LiFePO$_4$/C composite was then obtained by calcinating the organic filter templates at 600°C.

From the above experimental analysis, a possible mechanism of the formation of LiFePO$_4$/C replicas can be proposed as shown in Fig. 4. Two types of 1D channeled polycarbonate (P-100) and 3D interconnected meso- and macro-porous mixed-cellulose and cellulose (M-200 and C-700) were used as templates. Fig.4 shows the three major steps in the syntheses process: (i) infiltrating the LiFePO$_4$ precursor solution into the templates; (ii) heat-treatment of the impregnated template under a controlled atmosphere to respectively convert the organic template and precursor solution into residual carbon and amorphous LiFePO$_4$; (iii) removal of the template framework and crystallization of LiFePO$_4$ to form the LiFePO$_4$/C composites by calcination. In the final step, while the organic filter template was removed by calcination, the LiFePO$_4$ featured the nanofiber (P-100) and meso/macroporous (M-200 and C-700) structures with residual carbon from the decomposition of the organic template.

Due to the difficulty of synthesizing P-100 and extremely low yield of P-100, studies of this composite focused only on morphological analyses such as XRD, SEM and TEM. Thus, the following discussions regarding BET surface area and electrochemical tests will be limited to the M-200 and C-700 composites. The pore structure of the LiFePO$_4$/C produced from M-200 and C-700 was determined by nitrogen adsorption-desorption isothermal measurements. As shown in Fig. 5, the adsorption isothermal curve of the samples have a well-defined step as the typical IV classification with a H$_3$-type hysteretic loop in the p/p$_o$ range of 0.50 – 1.0, indicating mesoporous material character.
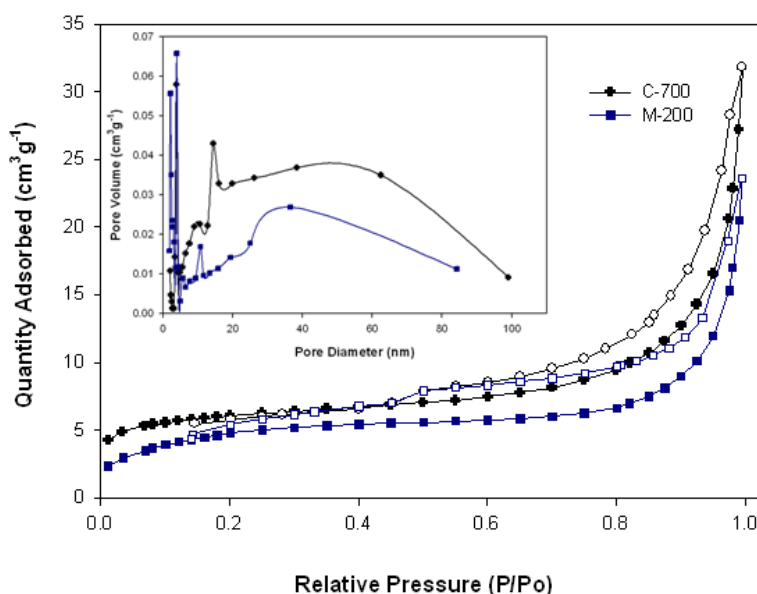
Figure 5. Nitrogen sorption isotherms for samples M-200 and C-700; filled and open markers respectively denote the adsorption and desorption branches of the isotherm. The insert is the BJH desorption pore size distribution.

The pore size distributions for both samples calculated from the adsorption branch of the isotherms based on BJH model, as shown in the insert of Fig.5. The result confirms the significant presence of mesopores for C-700. The pores prepared from the smaller template (M-200) may have partially broken down due to crystal growth thus reducing the pore volume. A similar occurrence was reported by Doherty *et al.* [41]. Therefore, the pore size is mainly a consequence of the micropores. These findings suggest that the $LiFePO_4$/C composite samples do not contain framework-confined pores but are rather made up of individual nanoparticles. This observation is also supported by the TEM images. Moreover, the BET specific surface area of M-200 and C-700 are respectively 18 and 24 m^2 g^{-1}. Generally, a larger surface area is important to improve the electrochemical performance of $LiFePO_4$ materials.

Table 2. EA, DLS, TEM, BET surface area, morphology, and discharge capacities for various samples.

Samples	Morphology	Carbon amount (wt%)	TEM Size (nm)	BET surface area (m^2/g)	Capacity at 0.1C rate (mAh/g)
P-100	nanofibers	0.79	150 nm	N/A	N/A
M-200	nanoparticles	2.3	70-200	18	135
C-700	nanoparticles	2.1	100-150	24	152

Table 2 lists the residual carbon content, morphology, BET specific surface area, morphology, and discharge capacity for various samples. The carbon content of the carbon coated $LiFePO_4$ in the as-prepared $LiFePO_4$/C composites was confirmed using an elemental analyzer (EA). The measured residual carbon content for all samples was about 0.79 ~ 2.3 wt%.
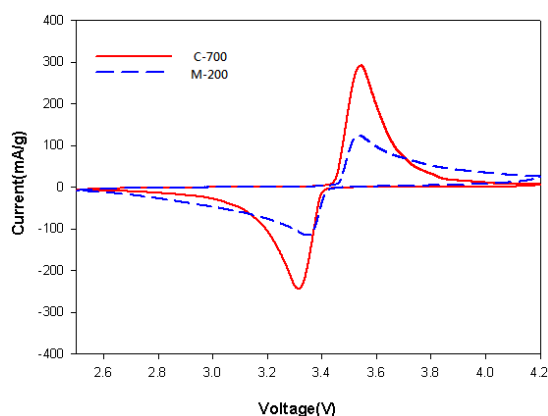
Figure 6. CVs of Li/1M $LiPF_6$, EC-DMC/$LiFePO_4$ cells were recorded during the 3rd cycle at a scanning rate of 0.1 mV s^{-1} for samples M-200 and C-700.

Fig. 6 represents the CV plots of the $LiFePO_4/C$ composites prepared from M-200 and C-700 cycled between 2.5 and 4.2 V at a scan rate of 0.1 mV s^{-1}. In the CV curves of both samples, the oxidation-reduction peaks of both samples appear between 3.5-3.6 V and 3.3-3.4 V, respectively, corresponding to the two-phase charge-discharge reaction of the Fe^{2+}/Fe^{3+} redox pairs at roughly 3.5 V. No other peaks were observed, suggesting the absence of electro-active iron impurities. According to the measurement of CV profiles (3rd cycle), both samples exhibit a similar coulombic efficiency of 98-99%. However, the peak intensities or discharge capacities are variable. The C-700 revealed a higher capacity than that with M-200.
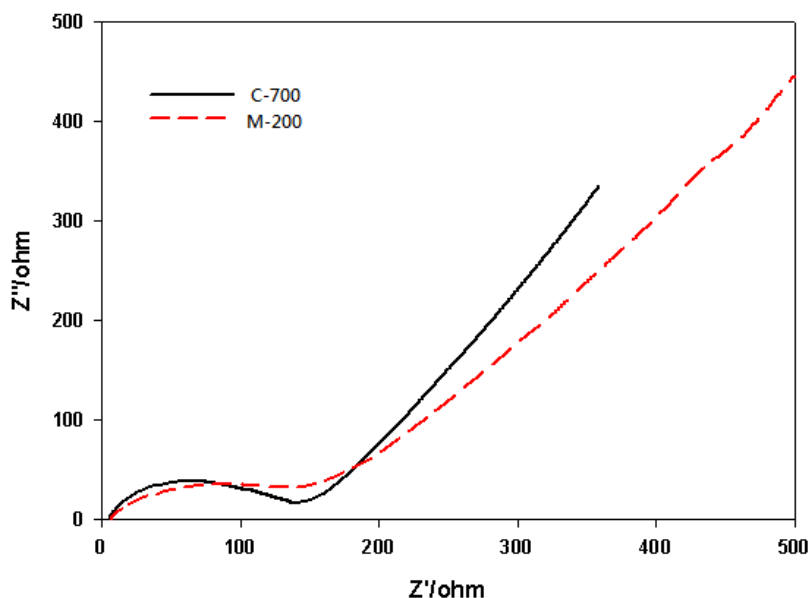

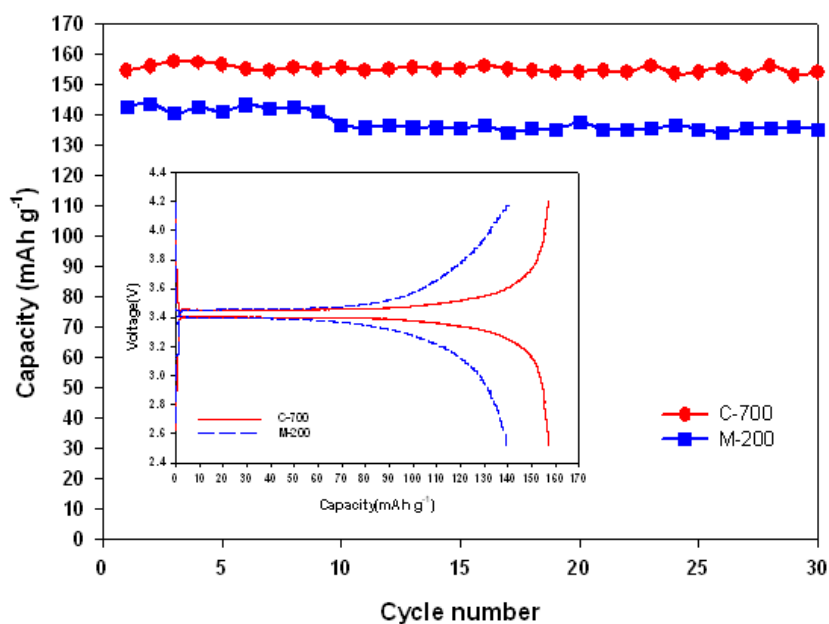**Figure 7.** AC impedance spectra of samples M-200 and C-700.


Figure 8. Capacity retention of the samples M-200 and C-700 cycled at 0.1C rate between 2.5 and 4.2 V. The insert shows the 5th charge/discharge curves.

The difference in cell capacity can be assigned to the higher surface area of C-700. Moreover, the difference in electrochemical performance is more obvious in ac impedance. The curves of electrochemical impedance spectra (EIS) present the typical Nyquist plot of the $LiFePO_4$/C prepared from M-200 and C-700, as shown in Fig. 7. The plot has a combination of a depressed semicircle in the medium-to-high frequency region and an inclined line in the low frequency region. The intercept at the Z' axis in the high frequencies region represents the ohmic resistance (R_e) of the electrolyte and the electrical contact. The semicircular plot in the medium frequency range is corresponding to the charge transfer resistance (R_{ct}) of the electrochemical reaction and the inclined line in the low frequency region represents the Warburg impedance, which related with Li^+ diffusion in the $LiFePO_4$/C particle. As represented in Fig.7, C-700 has a smaller charge transfer resistance ($R_{ct} \sim 135 \ \Omega$) and a larger diffusion of lithium ions than M-200 ($R_{ct} \sim 150 \ \Omega$). These results are in agreement with the high electrochemical performance of C-700 at a high discharge rate.

Fig. 8 plots capacity versus cycle number for the $LiFePO_4$/C prepared from M-200 and C-700. Both cells exhibit good discharge capacity retentions after 30 cycles. However, the C-700 capacity is significantly higher than the M-200 due to the increased presence of mesopores and greater surface area. The particle morphology and surface area are obvious to have a significant effect on electrochemical performance. The 5th charge-discharge voltage profiles of Li/$LiFePO_4$ cells for M-200 and C-700 at 0.1C rate between 2.5 and 4.2 V are shown the insert in Fig. 8. A wide flat charge-discharge plateau could be seen at approximately 3.4 V (vs. Li/Li^+), which implies that a two-phase Fe^{3+}/Fe^{2+} redox reaction proceeds via a first-order transition between $FePO_4$ and $LiFePO_4$. The small voltage difference between the charge-discharge plateaus demonstrates its good kinetics. The C-700 cell delivers a discharge capacity of 157 mAh g^{-1} in the 5th cycle, which corresponds to ~93% of the theoretical capacity of $LiFePO_4$ (170 mAh g^{-1}). The coulombic efficiency of all samples was at least 99%, which is in good agreement with the CV measurements.
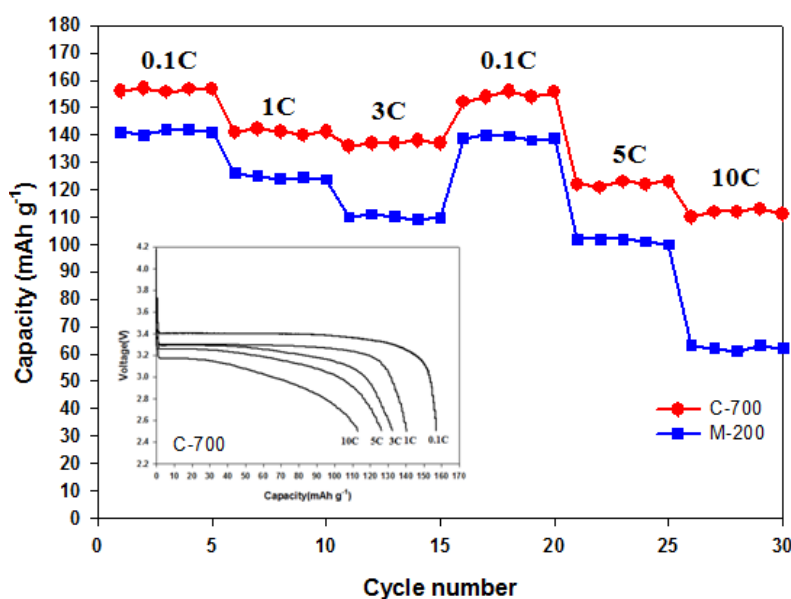
Figure 9. Cycle stability of samples C-700 and M-200 with various C rates. The insert is the charge/discharge curves of sample C-700 at different current rates.

Cycle stabilities of the cell at various discharge current rates are given in Fig. 9. At higher discharge rates, the C-700 has significantly higher capacities than the M-200. At a rate of 10C, a reversible capacity of 112 mAh g^{-1} can be achieved, which is ~ 71% of the initial capacity at 0.1C rate. This retention of the high rate capacity indicates the C-700 possesses an excellent rate capability and good cycle life, which can be attributed to the lower charge transfer resistance and greater diffusion of lithium ions for the C-700 materials. We find C-700 to be suitable for use as an organic filter template to produce a LiFePO$_4$/C composite with a good particle morphology and a uniformly coated carbon conductive layer, exhibiting better electrochemical performance. From the experimental results, the LiFePO$_4$/C composites prepared from appropriate organic templates have smaller particle sizes, larger specific surface areas, and highly uniform carbon distribution on the surface of the particles, which is consistent with the findings in other studies [10, 41, 42, 47-49, 51]. These characteristics provide composites with better electrochemical performance.

4. CONCLUSION

LiFePO$_4$/C composites were prepared using porous polycarbonate, mixed-cellulose, and cellulose as sacrificial hard templates. The nature of the organic filter templates was found to greatly affect the formation of the specific pore structure with various morphologies. Although the porosity of the C-700 (700 nm) cellulose template has a larger pore size, the LiFePO$_4$/C prepared from C-700 provides a uniform particle size within the 100-150 nm range, which can be ascribed to the effect of the structure of 3D fibers in the cellulose in dispersing the LiFePO$_4$ particles and reducing particle aggregations. The LiFePO$_4$/C prepared from the C-700 gave both high specific surface area and better access to the active LiFePO$_4$ material, thus this sample possesses a higher discharge capacity and better rate capability, with 157 mAh g^{-1} at 0.1C and 112 mAh g^{-1} at 10C. LiFePO$_4$/C powders synthesized from the appropriate organic filter templates clearly can provide excellent electrochemical performance.

References

1. J.B. Goodenough, Y. Kim, *Chem. Mater.*, 22 (2010) 587-603.
2. V. Aravindan, J. Gnanaraj, Y.-S. Lee, S. Madhavi, *J. Mater. Chem. A,* 1 (2013) 3518.
3. M. Park, X. Zhang, M. Chung, G.B. Less, A.M. Sastry, *J. Power Sources*, 195 (2010) 7904-7929.
4. M.M. Thackeray, C. Wolverton, E.D. Isaacs, *Energy Environ. Sci.*, 5 (2012) 7854.
5. K.F. Hsu, S.Y. Tsay, B.J. Hwang, *J. Mater. Chem.*, 14 (2004) 2690.
6. M. Li, L. Sun, K. Sun, S. Yu, R. Wang, H. Xie, *J. Solid State Electrochem.*, 16 (2012) 3581-3586.
7. [7] M.S. Whittingham, *Chem. Rev.*, 104 (2004) 4271-4301.

8.   J.W. Fergus, *J. Power Sources,* 195 (2010) 939-954.
9.   M.R. Yang, T.H. Teng, S.H. Wu, *J. Power Sources*, 159 (2006) 307-311.
10. S.C. Jheng, J.S. Chen, *Int. J. Electrochem. Sci.*, 8 (2013) 4901-4913.
11. J.H. Lin, J.S. Chen, *Electrochim. Acta,* 62 (2012) 461-467.
12. W.J. Zhang, *J. Power Sources*, 196 (2011) 2962-2970.
13. X. Sun, K. Sun, Y. Wang, X. Bai, C. Chen, B. Cui, *Int. J. Electrochem Sci,* 8 (2013) 12816-12836.
14. S. Yu, S. Dan, G. Luo, W. Liu, Y. Luo, X. Yu, Y. Fang, *J. Solid State Electrochem.*, 16 (2011)
     1675-1681.
15. C.W. Ong, Y.K. Lin, J.S. Chen, *J. Electrochem. Soc.*, 154 (2007) A527-A533.
16. Y.-F. Wu, Y.-N. Liu, S.-W. Guo, S.-N. Zhang, T.-N. Lu, Z.-M. Yu, C.-S. Li, Z.-P. Xi, *J. Power
     Sources,* 256 (2014) 336-344.
17. J. Mun, H.-W. Ha, W. Choi, *J. Power Sources,* 251 (2014) 386-392.
18. A. Naik, J. Zhou, C. Gao, L. Wang, *Int. J. Electrochem Sci*, 9 (2014) 6124-6133.
19. F. Croce, A. D' Epifanio, J. Hassoun, A. Deptula, T. Olczac, B. Scrosati, *Electrochem. Solid-State
     Lett.*, 5 (2002) A47.
20. K.S. Park, J.T. Son, H.T. Chung, S.J. Kim, C.H. Lee, K.T. Kang, H.G. Kim, *Solid State Commun.*,
     129 (2004) 311-314.
21. J. Liu, Z. Wang, G. Zhang, Y. Liu, A. Yu, *Int. J. Electrochem Sci,* 8 (2013) 2378-2387.
22. Y.W. Chen, J.S. Chen, *Int. J. Electrochem Sci*, 7 (2012) 8128-8139.
23. X. Yin, K. Huang, S. Liu, H. Wang, H. Wang, *J. Power Sources,* 195 (2010) 4308-4312.
24. M. Pan, X. Lin, Z. Zhou, *J. Solid State Electrochem.*, 16 (2011) 1615-1621.
25. H.C. Wang, J.R. Carey, J.S. Chen, *Int. J. Electrochem. Sci.,* 5 (2010) 1090-1102.
26. Y. Qiu, Y. Geng, J. Yu, X. Zuo, *J Mater Sci*, 49 (2014) 504-509.
27. K. Yang, Z. Deng, J. Suo, *J. Solid State Electrochem.*, 16 (2012) 2805-2813.
28. B.L. Ellis, K.T. Lee, L.F. Nazar, *Chem. Mater.*, 22 (2010) 691-714.
29. G. Kucinskis, G. Bajars, J. Kleperis, *J. Power Sources*, 240 (2013) 66-79.
30. Y. Hu, M.M. Doeff, R. Kostecki, R. Fiñones, *J. Electrochem. Soc.*, 151 (2004) A1279.
31. T. Nakamura, Y. Miwa, M. Tabuchi, Y. Yamada, *J. Electrochem. Soc.,* 153 (2006) A1108.
32. F. Caruso, *Adv. mater.*, 13 (2001) 11.
33. N.A. Dhas, K.S. Suslick, *J. Am. Chem. Soc.*, 127 (2005) 2368.
34. M.M. Doeff, Y. Hu, F. McLarnon, R. Kostecki, *Electrochem. Solid-State Lett.,* 6 (2003) A207.
35. Y. Vasquez, A.K. Sra, R.E. Schaak, *J. Am. Chen. Soc.*, 127 (2005) 12504.
36. P. Tierno, W.A. Goedel, *J. Phys. Chem.*,B, 110 (2006) 3043.
37. F. Schuth, *Angew Chem. Int. Ed.*, 42 (2003) 3604.
38. H. Xu, W. Wang, *Angew Chem. Int. Ed.*, 47 (2007) 1489.
39. A.H. Lu, F. Schuth, *CR Chimie*, 8 (2005) 609.
40. J.S. Sakamoto, B. Dunn, *J. Mater. Chem.,* 12 (2002) 2859.
41. C.M. Doherty, R.A. Caruso, B.M. Smarsly, C.J. Drummond, *Chem. Mater.*, 21 (2009) 2895-2903.
42. C.M. Doherty, R.A. Caruso, B.M. Smarsly, P. Adelhelm, C.J. Drummond, *Chem. Mater.,* 21
     (2009) 5300-5306.
43. J. Cabana, T. Valdés-Solís, M.R. Palacín, J. Oró-Solé, A. Fuertes, G. Marbán, A.B. Fuertes, *J.
     Power Sources,* 166 (2007) 492-498.
44. S. Lim, C.S. Yoon, J. Cho, *Chem. Mater.,* 20 (2008) 4560-4564.
45. J.Y. Luo, Y.G. Wang, H.M. Xiong, Y.Y. Xia, *Chem. Mater.,* 1*9* 4791-4795.
46. D. Jugović, M. Mitrić, M. Milović, B. Jokić, M. Vukomanović, D. Suvorov, D. Uskoković,
     Powder Technol., 246 (2013) 539-544.
47. Y. Wang, G. Cao, *Advanced Materials,* 20 (2008) 2251-2269.
48. T. Rao Penki, D. Shanmughasundaram, A.V. Jeyaseelan, A.K. Subramani, N. Munichandraiah, *J.
     Electrochem. Soc., 1*61 (2014) A33-A39.
49. P.G. Bruce, B. Scrosati, J.M. Tarascon, *Angew. Chem. Int Ed.*, 47 (2008) 2930-2946.

50. H.Y. Lin, S.M. Yeh, J.S. Chen, *Int. J. Electrochem Sc*i, 9 (2014) 6936-6948.
51. J. Hassoun, K.S. Lee, Y.K. Sun, B. Scrosati, *J. Am. Chem. Soc.*, 133 (2010) 3139-3143.
52. G.T.-K. Fey, H.-J. Tu, K.-P. Huang, Y.-C. Lin, H.-M. Kao, S.-H. Chan, *J. Solid State Electrochem.*, 16 (2012) 1857-1862.
53. Source:http://www.millipore.com/catalogue/item/vcwp09025 (accessed Jun 11, 2014).
54. laboratory filtration brochure 2013; GE Healthcare Life Science. http://www.gelifesciences.com/gehcls_images/GELS/Related%20Content/Files/1363086058160/lit doc29046171_20130428235059.pdf (accessed Jun 11, 2014).